NASA CONTRACTOR REPORT

NASA CR-1816

COMPUTATIONAL STUDIES OF THREE-DIMENSIONAL TRANSONIC SHEAR FLOW: WORK IN PROGRESS

by David A. Oliver and Panagiotis Sparis

Prepared by
GAS TURBINE LABORATORY
MASSACHUSETTS INSTITUTE OF TECHNOLOGY
Cambridge, Mass.
for Lewis Research Center

NATIONAL AERONAUTICS AND SPACE ADMINISTRATION • WASHINGTON, D. C. • MAY 1971

1. Report No. NASA CR-1816	2. Government Accession No.	3. Recipient's Catalog No.
4. Title and Subtitle COMPUTATIONAL STUDIES OF THREE-DIMENSIONAL TRANSONIC SHEAR FLOW: WORK IN PROGRESS		5. Report Date May 1971
		6. Performing Organization Code
7. Author(s) David A. Oliver and Panagiotis Sparis		8. Performing Organization Report No. GTL Report 101
		10. Work Unit No.
9. Performing Organization Name and Address Gas Turbine Laboratory Massachusetts Institute of Technology Cambridge, Massachusetts		11. Contract or Grant No. NGL 22-009-383
		13. Type of Report and Period Covered Contractor Report
12. Sponsoring Agency Name and Address National Aeronautics and Space Administration Washington, D.C. 20546		14. Sponsoring Agency Code
15. Supplementary Notes		

16. Abstract

The structure of three-dimensional transonic shear flow in a turbomachine cascade is examined in the context of a time dependent computer experiment. A transonic inlet Mach number profile along the span of the blade is incident on the cascade. This profile leads to the development of shocks located at the blade tip which weaken along the span of the blade and merge with the sonic surface. The static pressure rise across these tip shocks is effectively communicated across the passage to the hub end where it results in a deceleration of the hub flow which remains totally subsonic. The inlet stagnation pressure profile is manifested as a static pressure gradient at the blade leading edge which then induces strong cross flows along the span. The flow at the supersonic portion of the blade, however, expands to a much lower pressure than the pressure at the subsonic hub end so that this cross flow eventually reverses back towards the tip near the trailing edge.

17. Key Words (Suggested by Author(s)) Transonic shear flow; Compressors; Three-dimensional flow; Turbomachine cascade	18. Distribution Statement Unclassified - unlimited

19. Security Classif. (of this report)	20. Security Classif. (of this page)	21. No. of Pages	22. Price*
Unclassified	Unclassified	36	$3.00

*For sale by the National Technical Information Service, Springfield, Virginia 22151

FOREWORD

The research described in this report was conducted at the MIT Gas Turbine Laboratory under NASA grant NGL 22-009-383. Dr. John C. Evvard of the Lewis Research Center was the NASA Project Manager. The report was originally issued as MIT GTL report 101.

CONTENTS

1. INTRODUCTION

In the present study, the structure of the three dimensional transonic shear flow is examined in the context of a time dependent computer experiment. The specific problem studied is that of flow through a linear cascade of blades at zero angle of attack to the incident flow. The three dimensional features of the flow are introduced by the presence of a volocity nonuniformity along the span direction in the incident flow. This spanwise velocity profile is manifested as a spanwise Mach number profile; and this Mach number profile is taken to be transonic possessing a subsonic region at one end of the span (e.g. the hub) and a supersonic region at the opposite end of the span (e.g. the tip). Such a flow possesses certain features which are characteristic of the flow incident on a transonic turbomachine rotor.

2. TRANSONIC FLOW IN A TURBOMACHINE CASCADE

The problem of three dimensional transonic shear flow is, in many senses, a classic problem. It follows directly as an extension of a classic problem which is already understood in considerable detail: that of two dimensional (span-wise uniform) transonic flow over an airfoil or turbomachine blade.

For the two dimensional case it is known that as the incident Mach number is steadily increased in the subsonic range a critical Mach number is reached at which the flow becomes sonic at some point on the blade. As the Mach number is further increased, a supersonic region appears (enveloped by the sonic bubble). For most shapes, as the Mach number increases this supersonic region is terminated by a concave forward shock. As the Mach number increases further the terminating shock moves rearward until, as the Mach number slightly exceeds unity (supersonic incident flow) the rearward shock stands at the trailing edge and a shock develops at the leading edge. This structure is confirmed by numerous experiments (which also reveal the shock boundary layer interaction) and by a remarkable tradition of analysis beginning with the classical work of the Hodograph(1) extending over the numerical finite difference work of Emmons(2) and the non-linear theory of Rubbert and Landahl.(3)

The extension of this problem to a three dimensional archetypal problem results from the following change of condition. The inlet flow is now allowed to develop a velocity gradient along the span of the blade which generates a span-wise nonuniform Mach number profile. This inlet Mach number profile will itself be transonic possessing both supersonic and subsonic regions. In such a three dimensional transonic regime, the structure of the sonic surface, shock surface, and induced cross flows are of particular interest. Such a flow models in many respects the relative Mach number profile which is incident on a transonic turbomachine rotor.

In contrast to two dimensional flows, three dimensional transonic flows have received little theoretical attention. The linearized non-lifting transonic cascade theory was developed by McCune(4) in 1958 and recently extended to the lifting case by Okurounmu and McCune.(5) The recent work of Namba(6) proceeds from linearized theory to construct solutions for transonic shear flow over an airfoil. The most significant result of this work was the development of complex patterns of standing waves on the blade near the sonic spanwise stations. There remains in this work, however, the fundamental limitation of linearized theory: the shock structure cannot be represented.

3. METHODS FOR THE CALCULATION OF INVISCID TRANSONIC FLOW

The systematic numerical study of inviscid compressible flow was first developed by Courant, Friedrichs, and Lewy(7) and Lax and Wendroff.(8) These methods are time dependent initial value methods for hyperbolic fluid equations in the sense that an initial fluid state is advanced in time subject to prescribed boundary conditions in space. For situations in which only the steady flow subject to time independent boundary conditions is required, the initial value method may be used to develop this steady flow from an initial guess. The desired steady flow is then obtained as the asymptotic state for large values of time.

It is necessary that weak solutions of the fluid equations be represented by the methods i.e., that shock surfaces separating regions of elliptic and hyperbolic behavior be permitted. The methods utilized in this work are of this variety. Shock surfaces are located internally. It is not necessary to match elliptic and hyperbolic regions at an a priori unknown surface using the Rankine-Hugoniot conditions. Instead, the shock becomes a sharply varying (but continuous) region in which the shock is dispersed over 3-4 computing mesh cells.

It should be noted that several other difference methods exist for integrating the inviscid compressible flow equations. These methods include those of Rusanov,[9] Von Neumann,[10] and others. In the class of problems in which we are interested the resolution of sonic surfaces and weak shock waves is of extreme importance. The resolving capability of the method is therefore of major interest. Emery[11] has compared the resolution offered by several of the methods described above. His results showed that the Lax-Wendroff method (in either its original or two-step form) offered the best resolution of the flow field of all the methods. The Lax-Wendroff method in its two-step version [Richtmyer[12]] was therefore utilized in the present work.

The description of the two-step version of the Lax-Wendroff method is given in considerable detail by Richtmyer[12]. We remark that the method is of second order accuracy in time and note that the numerical stability of the method is essentially governed by a limitation on time step Δt given by the Courant condition:

$$\Delta t \lesssim \min \left\{ \frac{\Delta x}{|u| + c} \right\}$$

where Δx is the spatial size of a mesh cell and c and u are the local sonic and fluid speeds respectively. The above result is obtained from a linearized stability analysis of the Lax-Wendroff difference equations. This analysis also shows that the Lax-Wendroff method is neutrally stable in a numerical sense at a sonic point or at a stagnation point. This fact suggests that numerical instabilities could arise in a transonic calculation where there are significant regions near the sonic speed. This has been found to be the case. When the Lax-Wendroff method was used for the transonic airfoil problem, slowly growing instabilities were observed. This situation may be corrected by adding to the Lax-Wendroff equations an artificial diffusion term which is of third order in the time step and therefore does not affect the truncation error of the scheme [Burstein,[13] Lapidus[14]]. This small diffusion term is sufficient to render the otherwise neutrally stable method stable in sonic or near sonic regions.

Because of our interest in the three dimensional problem, the conservation of computer execution time and memory becomes of importance. This general consideration requires that each mesh point be used effectively. In the case of flows over bodies, the strongest gradients are near and on the body so that it seems reasonable to have most of the mesh points in the vicinity of and on the body while fewer mesh points may be tolerated at larger distances from the body. For the present class of problems, we have developed a mapping procedure for allocation of the mesh in which the physical domain is mapped one to one into a solution domain which is then uniformly discretized. The mapping function is selected so that the uniform mesh in the solution domain maps into the physical domain with a greater number of points in the region where maximum resolution is desired. Further details of this mapping technique may be found in Sparis.[15]

4. FLUID EQUATIONS AND THEIR DIFFERENCE FORMULATION

The formulation of the problem is centered on the geometry of fig.1. The blade of chord 2ℓ, thickness t and span D is suspended in the center of a rectangular passage. In the problem to be discussed, the blade is symmetric and parallel to the incident stream. With this symmetry, the walls parallel to the span may simply be interpreted as fictitious symmetry boundaries for a linear cascade. The inlet flow possesses uniform static thermodynamic properties at the inlet, but a linearly varying velocity profile in the z direction along the span. The fluid equations utilized are those for inviscid compressible flow and the boundary conditions on the surface of the blade are those for inviscid flow: vanishing normal velocity at the surface. The inlet state is prescribed as discussed above. There appear to be a variety of ways to model the exit boundary depending on the kind of situation one is attempting to computationally simulate. For the case of a single isolated rectilinear cascade one should apply the upstream (inlet) and downstream (exit) boundary condition at $+\infty$, $-\infty$ respectively. Although it is possible to map this infinite domain into a finite domain, and then carry out the numerical work in the finite domain, it has been found adequate in many cases to simply locate inlet and exit far enough upstream and downstream so that the flow can be specified to be uniform in the axial direction e.g. Burstein.[13] That is the procedure initially adopted in this work although it may require modification for situations in which shocks escape from the cascade. It appears feasible in such an event to adjust the exit boundary condition so that the reward characteristics are properly located at the exit.

For a perfect gas of mass density ρ, momentum density in rectangular coordinate directions x,y,z, given by m_x, m_y, m_z, and total energy density e, the inviscid, compressible fluid equations may be expressed as

$$\frac{\partial \vec{U}}{\partial t} + \frac{\partial \vec{F}}{\partial x} + \frac{\partial \vec{G}}{\partial y} + \frac{\partial \vec{H}}{\partial z} = 0 \tag{1}$$

where $\vec{U}$ is the fluid state vector

$$\vec{U} = \begin{bmatrix} \rho \\ m_x \\ m_y \\ m_z \\ e \end{bmatrix} \tag{2}$$

and $\vec{F}, \vec{G}. \vec{H}$ are functions of $\vec{U}$:

$$\vec{F}(\vec{U}) = \begin{bmatrix} m_x \\ m_x^2/\rho + p \\ m_x m_y/\rho \\ m_x m_z/\rho \\ (e+p)m_x/\rho \end{bmatrix} \qquad \vec{G}(\vec{U}) = \begin{bmatrix} m_y \\ m_x m_y/\rho \\ m_y^2/\rho + p \\ m_z m_y/\rho \\ (e+p)m_y/\rho \end{bmatrix} \tag{3}$$

$$\vec{H}(\vec{U}) = \begin{bmatrix} m_z \\ m_x m_z/\rho \\ m_y m_z/\rho \\ m_z^2/\rho + p \\ (e+p)m_z/\rho \end{bmatrix}$$

The pressure p for a perfect gas is given by

$$p = (\gamma - 1)\left(e - \frac{m_x^2 + m_y^2 + m_z^2}{2\rho}\right) \tag{4}$$

where γ is the ratio of specific heats.

If space and time are discretized by increments $\Delta x, \Delta y, \Delta z; \Delta t$ with discrete coordinates j, ℓ, m, n such that $x = j\Delta x$, $y = \ell\Delta y$, $z = m\Delta z$, $t = n\Delta t$ and $\vec{U}^n_{j,\ell,m}$ denotes $\vec{U}(x,y,z,t)$, the two step Richtmyer version of the Lax-Wendroff scheme[12] is:

$$\begin{aligned}\vec{U}^{n+1}_{j,\ell,m} = {} & (\vec{U}^n_{j+1,\ell,m} + \vec{U}^n_{j-1,\ell,m} + \vec{U}^n_{j,\ell+1,m} + \vec{U}^n_{j,\ell-1,m} + \vec{U}^n_{j,\ell,m+1} + \vec{U}^n_{j,\ell,m-1})/6 \\ & - \frac{\Delta t}{2\Delta x}\left(\vec{F}^n_{j+1,\ell,m} - \vec{F}^n_{j-1,\ell,m}\right) \\ & - \frac{\Delta t}{2\Delta y}\left(\vec{G}_{j,\ell+1,m} - \vec{G}_{j,\ell-1,m}\right) \\ & - \frac{\Delta t}{2\Delta z}\left(\vec{H}_{j,\ell,m+1} - \vec{H}_{j,\ell,m-1}\right)\end{aligned} \tag{5a}$$

$$\begin{aligned}\vec{U}^{n+2}_{j,\ell,m} = \vec{U}^n_{j,\ell,m} & - \frac{\Delta t}{\Delta x}\left(\vec{F}^{n+1}_{j+1,\ell,m} - \vec{F}^{n+1}_{j-1,\ell,m}\right) \\ & - \frac{\Delta t}{\Delta y}\left(\vec{G}^{n+1}_{j,\ell+1,m} - \vec{G}^{n+1}_{j,\ell-1,m}\right) \\ & - \frac{\Delta t}{\Delta z}\left(\vec{H}^{n+1}_{j,\ell,m+1} - \vec{H}^{n+1}_{j,\ell,m-1}\right)\end{aligned} \tag{5b}$$

As discussed by Lax[8] and Richtmyer,[12] the above difference scheme is stable to small disturbances if

$$\Delta t \leqslant \frac{1}{\sqrt{3}} \; \frac{\Delta x}{|u|+c} \tag{6}$$

where $\Delta x = \Delta y = \Delta z$. For unequal space increments, the above stability condition is modified slightly [See Sparis[9]], however, for practical purposes, a working stability requirement is

$$\Delta t \leqslant \frac{1}{3} \min \left\{ \Delta/|u| + c \right\} \tag{7}$$

where Δ is the minimum spatial mesh increment.

In addition, the scheme is neutrally stable to small disturbances in regions where $u = 0$ or $u = a$; i.e., at stagnation points or sonic points. To stabilize the scheme against higher order disturbances, an artificial diffusion term which is of the order of the truncation error is added to the basic two step difference scheme. This term has been taken as an extended version of that proposed by Lapidus:[14]

$$\vec{V}_{j,\ell,m} = \frac{\kappa\Delta t}{\Delta x}\left[\left|u^n_{x_{j+1,\ell,m}} - u^n_{x_{j,\ell,m}}\right|\left(\vec{U}^n_{j+1,\ell,m} - \vec{U}^n_{j,\ell,m}\right) - \left|u^n_{x_{j,\ell,m}} \quad u^n_{x_{j-1,\ell,m}}\right|\left(\vec{U}^n_{j,\ell,m} - \vec{U}^n_{j-1,\ell,m}\right)\right]$$

$$+ \frac{\kappa\Delta t}{\Delta y}\left[\left|u^n_{y_{j,\ell+1,m}} - u^n_{y_{j,\ell,m}}\right|\left(\vec{U}^n_{j,\ell+1,m} - \vec{U}^n_{j,\ell,m}\right) - \left|u_{y_{j,\ell,m}} - u^n_{y_{y,\ell-1,m}}\right|\left(\vec{U}^n_{j,\ell,m} - \vec{U}^n_{j,\ell-1,m}\right)\right]$$

$$+ \frac{\kappa\Delta t}{\Delta z}\left[\left|u^n_{z_{j,\ell,m+1}} - u_{z_{j,\ell,m}}\right|\left(\vec{U}^n_{j,\ell,m+1} - \vec{U}^n_{j,\ell,m}\right) - \left|u_{z_{j,\ell,m}} - u_{z_{j,\ell,m-1}}\right|\left(\vec{U}^n_{j,\ell,m} - \vec{U}^n_{j,\ell,m-1}\right)\right] \qquad (8)$$

In the above u_x, u_y, u_z are the three components of the fluid speed and κ is a non-dimensional adjustable parameter of order unity. The term $\vec{V}^n_{j,\ell,m}$ is added to the right hand side of Eq.(5b).

As noted previously, the inlet boundary condition at $x = x_i$ is that of a specified inlet state $\vec{U}(x_i, y, z, t)$. At the exit far downstream, $x = x_e$ the condition of axial uniformity is applied:

$$\frac{\partial \vec{u}}{\partial x} = 0 \qquad x = x_e$$

On the surface of the blade which is parallel to the z axis, there must be no transport of mass, momentum, or energy across that surface. Although it is not an essential simplification, it is useful to use the approximation of thin airfoil theory and apply the blade boundary condition on the axis $y = 0$. Mappings or interpolation represent alternative procedures which allow exact application of the boundary conditions at the blade surface. In the present study, the specific blade profiles which were examined were 8% thick parabolic profiles. The thin airfoil approximation was compared with a mapping procedure which exactly treated the thickness problem; for the 8% thick profiles, there was no detectable difference between the two procedures. The thin airfoil treatment was therefore used in the results discussed in the present report.

Denoting normal and tangential directions by n,t on the blade surface, the surface conditions are:

$$
\begin{aligned}
&m_n = 0 && \text{(normal mass)} \\
&\frac{m^2}{\rho}{}_n = 0 && \text{(normal momentum)} \\
&m_n \frac{m}{\rho}{}_t = 0 && \text{(tangential momentum)} \\
&m_n \frac{e}{\rho} = 0 && \text{(total energy)}
\end{aligned}
\tag{9}
$$

If the values at mesh points in a rectangular x, y grid on either side of the blade interface are denoted (+),(-) superscripts (fig.2) the above conditions may be specified as

$$
\begin{aligned}
\rho^- &= \rho^+ \\
e^- &= e^+ \\
m_x^- &= m_x^+ \cos(2\theta) + m_y^+ \sin(2\theta) \\
m_y^- &= m_x^+ \sin(2\theta) - m_y^+ \cos(2\theta)
\end{aligned}
\tag{10}
$$

where θ is the angle between the y axis and the local normal at the blade surface. These conditions serve to fix the exterior boundary values (-) in terms of the interior values (+).

Because of interest in minimizing the number of mesh points for a given resolution, a mapping procedure was used to improve the resolution near the blade. Since the flow is principally axial with strong axial gradients, the x coordinate was stretched according to the following mapping:

$$(x,y,z) \rightarrow (\xi,y,z)$$
$$d\xi = \mu dx$$

where $\mu \equiv \psi / \langle\psi\rangle$ and $\psi(x)$ is a magnification function which has a maximum at $x = x_o$ and is monotone decreasing for $|x| < x_o$. The average value $\langle\psi\rangle$ is

A simple and useful magnification function is the "Lorentz Line Shape" function

$$\psi(x) = \frac{1}{1 + \left(\frac{x - x_o}{a}\right)^2} \tag{11}$$

where the parameter a is the value of x where $\psi(x)$ has the value 1/2. The domain (ξ,y,z) becomes the solution domain which is uniformly discretized, and hence, the mesh will be nonuniform in the x direction with a greater mesh point density in the region $x = x_o$. It should be noted that the stability requirement of the difference scheme must still be based upon the minimum physical spatial increment, Δx . The only required change in the fluid equations and their corresponding difference equations is the replacement of $\frac{\partial}{\partial x}$ by $\left(\frac{d\xi}{dx}\right)\frac{\partial}{\partial \xi}$

To give an illustration of the behavior of the transformation, for the parameter choices $a=3.71$, $L=26.0$, $x_o=0$, $\ell=3.71$ the maximum magnification factor μ is 2.71 and the blade will have 2.12 times as many points as it would with a uniform mesh in the x space. The correspondence between the solution space (ξ) and the physical space (x) is shown in fig.3.

5. TWO DIMENSIONAL RESULTS

Before proceeding to the three-dimensional problem, a two-dimensional subcase of the general formulation (span-wise uniform inlet velocity) was examined. The goal was to gain experience with resolution, stability, and accuracy in the two-dimensional case. The specific case chosen was uniform inlet flow over an 8% thick parabolic blade. The initial state was a uniform flow throughout the domain identical with the inlet flow, the inlet flow initially at Mach number $M_o=0.65$. As time progressed, the inlet Mach number was increased to 0.70, 0.75, 0.80, 0.84. The results of this time-dependent computer experiment are shown in figs. 4 through 7 . Full details may be found in Sparis.[15] These results lead to the following general conclusions:

1. The crucial flow field features of interest in this general problem -- sonic line and shock line -- could be resolved quite satisfactorily with a minimum discretization of the domain. These calculations were carried out with an intentionally coarse grid in anticipation of the more demanding requirements of storage and speed for a three dimensional calculation. The axial direction is represented by 40 mesh points, 27 of which are located on

the blade. Since the shock is dispersed over 3-4 mesh points, the shock thickness is of the order of slightly more than 10% of the chord. While one would prefer better, this resolution is adequate to quite clearly identify the phenomenon as a shock and locate the center of the dispersed region (figs.5,7). A separate application of the Rankine-Hugoniot conditions on either side of the shock shows them to be satisfied to the accuracy of the discretization error in the calculation. A calculation of the entropy of the flow field shows it constant on either side of the shock with the proper jump across the shock. Since there always exists a region within the shock where the Mach Number is unity, the rear portion of the sonic line (fig.6) also shows the shock location quite clearly.

2. The near neutral stability of the Lax-Richtmyer method in the transonic regime requires the use of a higher order diffusion term to provide numerical stabilization. It appears that this term may have some effect in introducing a slight distortion in the symmetry of the flow (especially evident in the shockless flow cases shown in fig.4). The elimination of this slight streamline distortion is currently being investigated.

3. The mesh allocation system based on a mapping seems to be satisfactory. Although the blade is only 1/5 of the axial passage length, approximately 60% of the mesh points were located on the blade where the gradients were strongest.

6. THREE DIMENSIONAL RESULTS

The initial flow for the three dimensional experiment was a span-wise uniform inlet flow at inlet Mach number 0.65. For the 8% thick parabolic profile at this Mach number the flow over the entire blade is subsonic. At the initial time the inlet flow is slowly sped up along the span with a linear velocity variation along the span. The span-wise nonuniformity is thus introduced continuously rather than discontinuously as time proceeds. In this way the development of the three-dimensional features of the flow from the purely two-dimensional flow may be observed as time proceeds. In the experiment to be described, the inlet velocity profile develops until the Mach number reaches a maximum value of 1.2 at the tip end of the blade. The Mach number at the hub remains fixed at 0.65. The time scale for the development of the profile is 1 blade chord crossing time for a sound wave at the inlet temperature.

Some preliminary results of this three-dimensional computer experiment are shown in the sequence of figures 8 through 21 . Each figure corresponds to an interval of 100 cycles which in turn corresponds to one chord crossing time at the inlet sonic speed at the hub. The sequence begins 300 cycles after the initiation of the inlet speed-up [fig. 8] and runs to 1100 cycles [fig. 16]. At 1100 cycles the flow is very close to its final asymptotic steady state as can be seen in fig. 21 .

At 300 cycles, the entire flow field is still subsonic, but the tip of the blade is beginning to show the effect of the spanwise nonuniformity. The maximum Mach number in the vicinity of the blade at this stage of the evolution of the flow is 0.93 and it occurs near the mid-chord point at the tip. After 300 cycles, the tip station possesses a region of supersonic flow. After 500 cycles, the maximum Mach number on the blade is 1.15 and is still at the tip. The point of maximum Mach number now begins to shift to the rear of the profile. At 500 cycles, the Mach number profiles steepens at the rear of the blade tip and by 600 cycles a weak shock surface is in evidence at the tip. This shock surface which intersects the blade weakens along the span running from tip to hub and merges with the sonic surface which intersects the span about two-thirds of the distance from hub to tip. Once the shock forms, the static pressure rise at the tip end of the passage is rapidly communicated across the passage to the hub end. This high back pressure on the streamlines at the hub end begins to decelerate the hub flow (which is still subsonic) as can be seen by the steady hub Mach number decrease from about 400 cycles. In fact, the hub flow accelerates steadily in response to the inlet speedup until about 400 cycles when the tip shock forms. From the onset of the tip shock, the hub flow steadily decelerates. By 1100 cycles, the hub exit Mach number is significantly less than the hub inlet Mach number.

At 1100 cycles the tip shock has strengthened and spread over half the blade span. From about 400 cycles, the incident flow at the leading edge of the tip is supersonic and hence the Mach number profile at the leading edge steepens forming a weak leading edge shock. Because of the poor resolution in the vicinity of the sharp leading edge, the leading edge shock is not as well represented as the rear shock.

It should be noted that once mixed flow exists in the vicinity of the blade, the Mach number profiles begin to develp fine scale wave-like patterns. It may well be that these are the long wavelength components of the complex steady wave structures which were predicted from linearized theory by Namba.(6)

The cross flow and static pressure distribution in the plane of the blade at 1100 cycles are shown in figs. 19 and 20 . In general, the cross flow may be interpreted in terms of the static pressure gradients. The inlet stagnation pressure profile is manifested as a static pressure profile at the leading edge of the blade and a strong cross flow from tip to hub is set up in this region. Since the flow at the supersonic tip expands over the blade to much lower back pressure than the subsonic hub flow, this leading edge cross flow is eventually reversed towards the rear of the chord where the tip static pressure falls below the hub static pressure. The cross flow reverses at this point and flows back towards the tip. After the shock, however, there is a slightly higher static pressure near the tip which again reverses the cross flow in the direction of the hub.

Perhaps the most remarkable feature of this experiment is the striking fact that the three-dimensional features of the flow field appear very much like a set of weakly interacting two-dimensional strips. Perhaps this is because the span length is rather small compared to the blade period (1/2.7) and this imposes a rather strong tendency for two-dimensional behavior. The inlet Mach number profile in the present calculation was rather strong in spanwise gradient. One suspects that for more "transonic" inlet profiles (e.g. $M_{hub} = 0.95$, $M_{tip} = 1.05$) more complex surface Mach number profile behavior would result as the flow engaged the subsonic region characteristic of the hub and the supersonic Ackeret profiles characteristic of the tip. A second noteworthy feature is the existence of the shock surface near the tip. There has been some speculation that the three-dimensional relief provided by a spanwise nonuniformity would relieve the necessity of hyperbolic elliptic transition through a compression discontinuity. This appears not to be the case.

REFERENCES

1. Lighthill, M.J., "The Hodograph Transformation in Trans-sonic Flow," Proc. Roy. Soc. (A), 191 (1947).

2. Emmons, H., "The Numerical Solution of Compressible Fluid Flow Problems," NACA Tech. Note, No. 932 (1944).

3. Rubbert, P. and Landahl, M., AIAA Journal 5, 3, p. 470 (1967).

4. McCune, J.E., "The Transonic Flow Field of an Axial Compressor Blade Row," Journ. Aero. Sci., 25, pp. 616-626, 1958.

5. Okurounmu, O. and McCune, J.E., AIAA Journal 8, pp. 1275-1283 (1970).

6. Namba, M., J. Fluid Mech., Vol. 36, Part 4, p. 759-783 (1969).

7. Courant, R., Friedrichs, K., and Lewy, H., Math. Amn., 100, p. 32 (1968).

8. Lax, P. and Wendroff, B., Comm. Pure Appl. Math., Vol. 13, p. 217 (1960).

9. Rusanov, V., "Calculation of Interaction of Non-Steady Shock Waves with Obstacles," Kat. Res. Council, Canada, Trans. 1027 (1962).

10. Von Neumann, J. and Richtmyer, R., J. Appl. Phys., 21, 3, p. 232 (1950).

11. Emery, A., J. Comp. Phys., 2, p. 306 (1968).

12. Richtmyer, R. and Morton, H., Difference Methods for Initial Value Problems, Wiley: New York (1967).

13. Burstein, S., "Numerical Calculations of Multidimensional Shocked Flows," Courant Institute of Mathematics, Rept. NYO Y 480-33 (1965).

14. Lapidus, A., J. Comp. Phys., 2, p. 154-177 (1967).

15. Sparis, P., The Numerical Calculation of Two-Dimensional Transonic Flow, S.M. Thesis, Mass. Inst. of Tech., June, 1970.

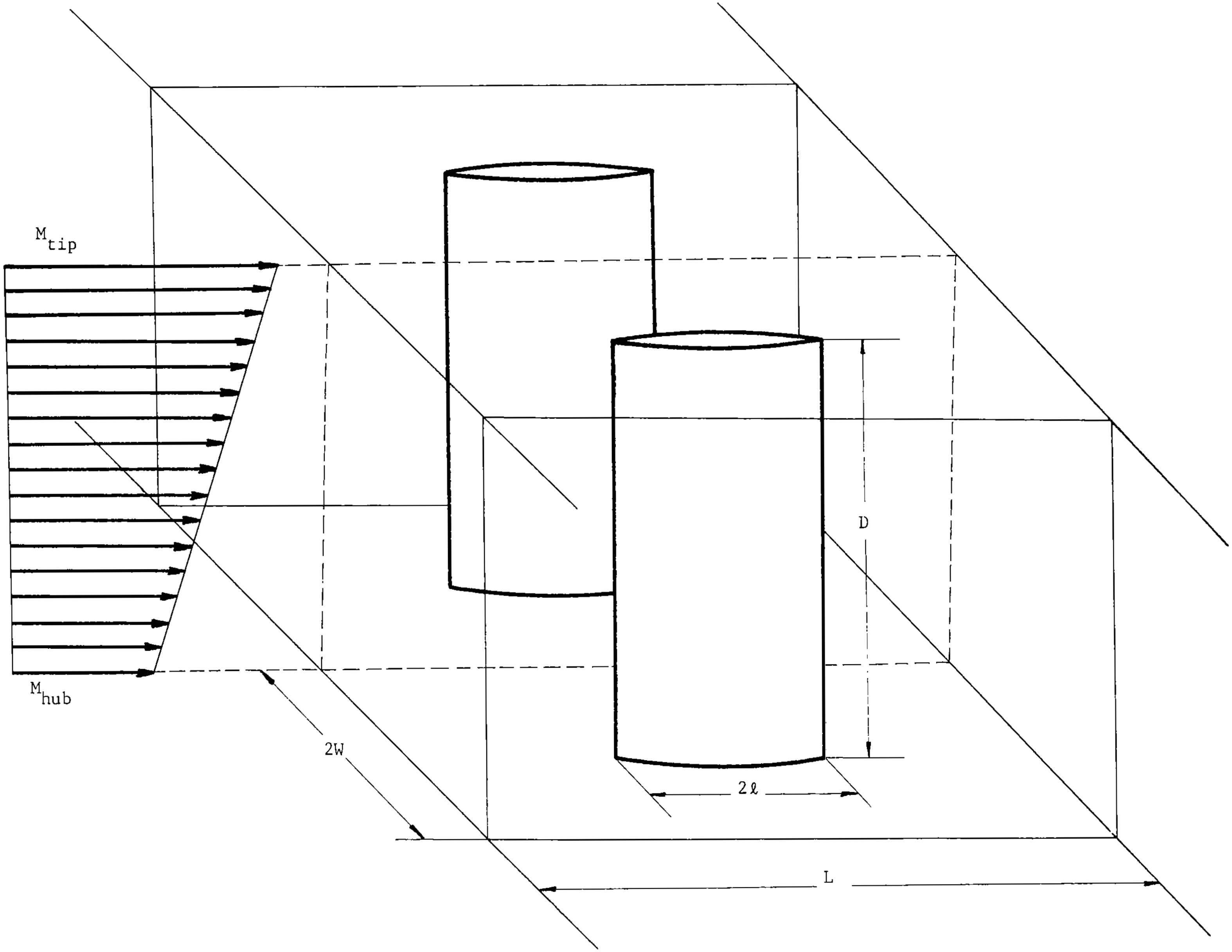

Figure 1. Cascade and flow field configuration.

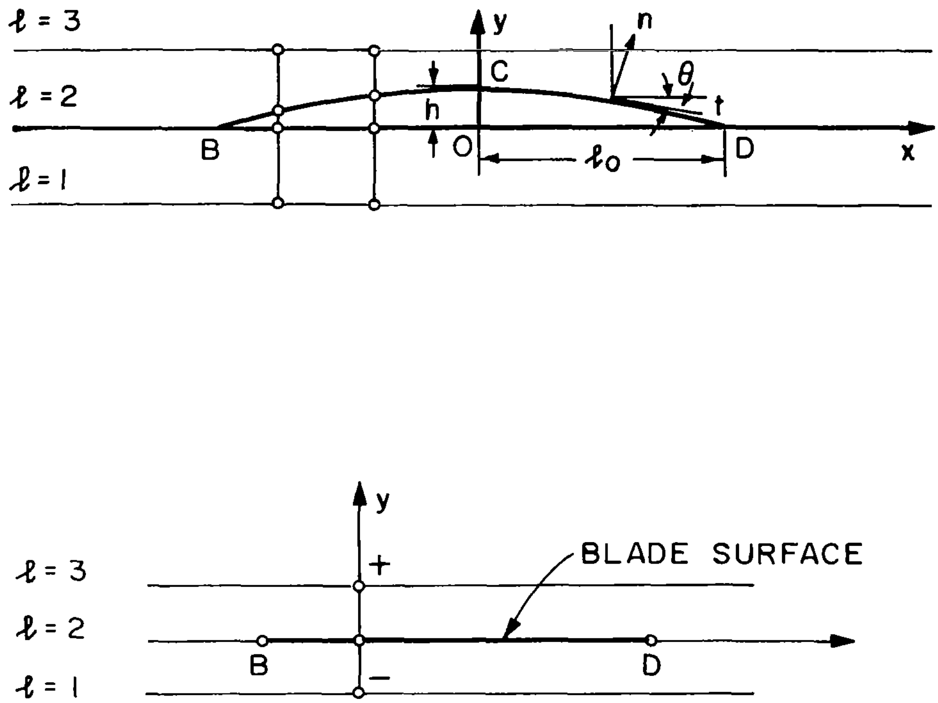

Figure 2.

Boundary conditions and mesh points at blade surface.

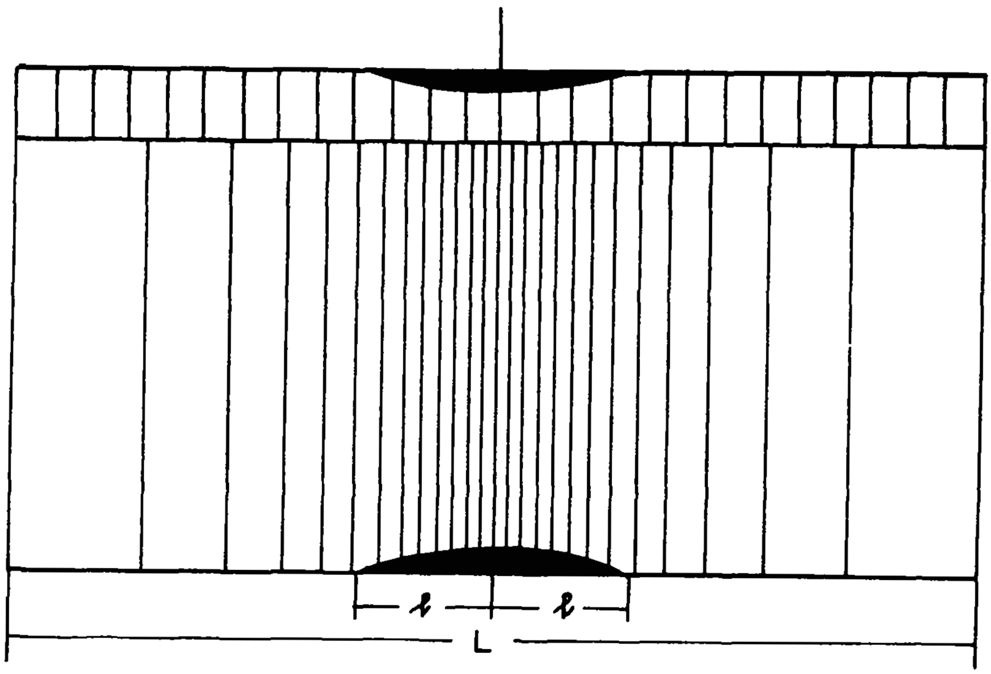

Figure 3.

Physical domain and solution domain correspondence.

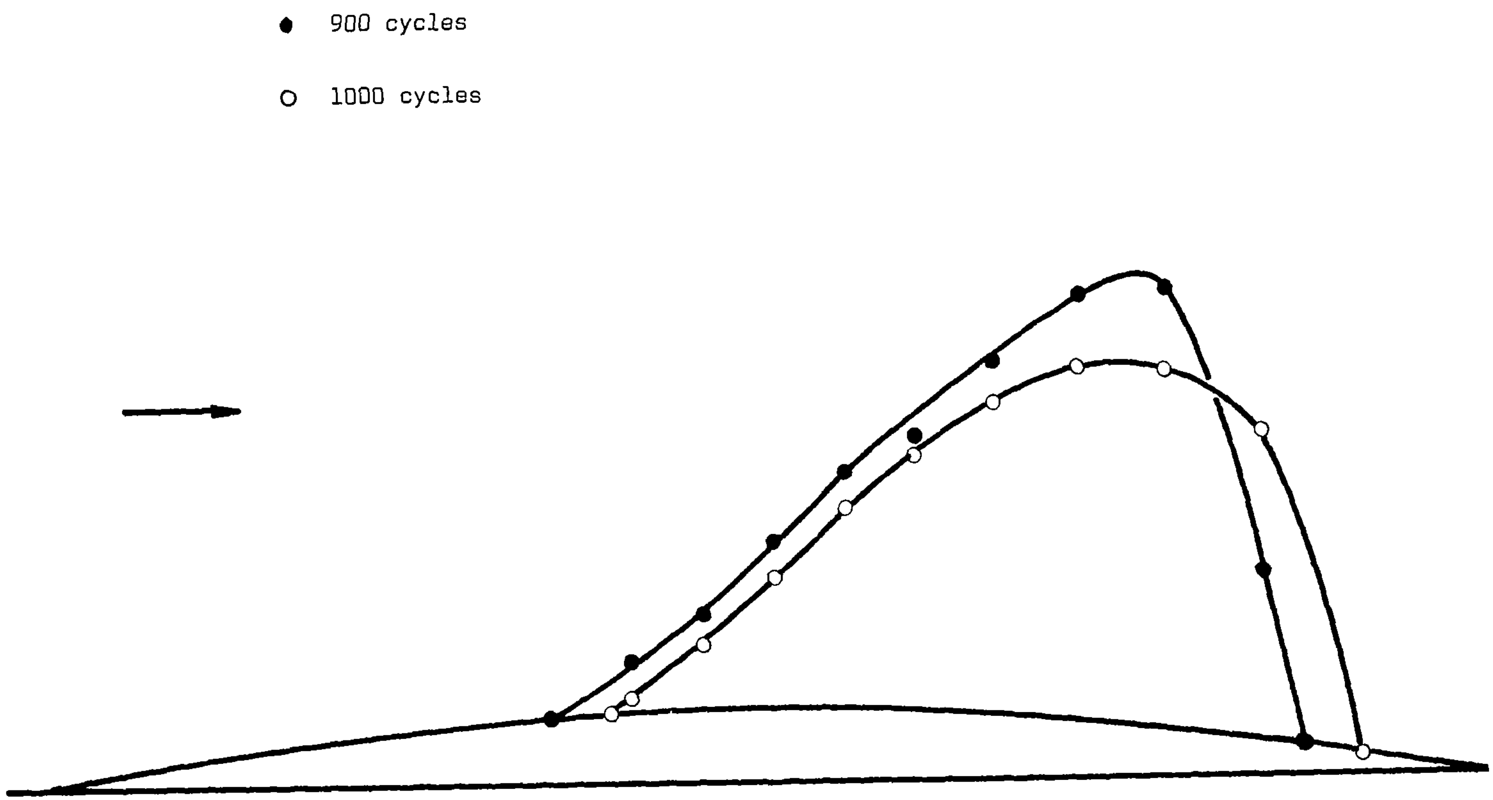

Figure 4. Sonic line development in two-dimensional time varying flow. $M_o = 0.84$.

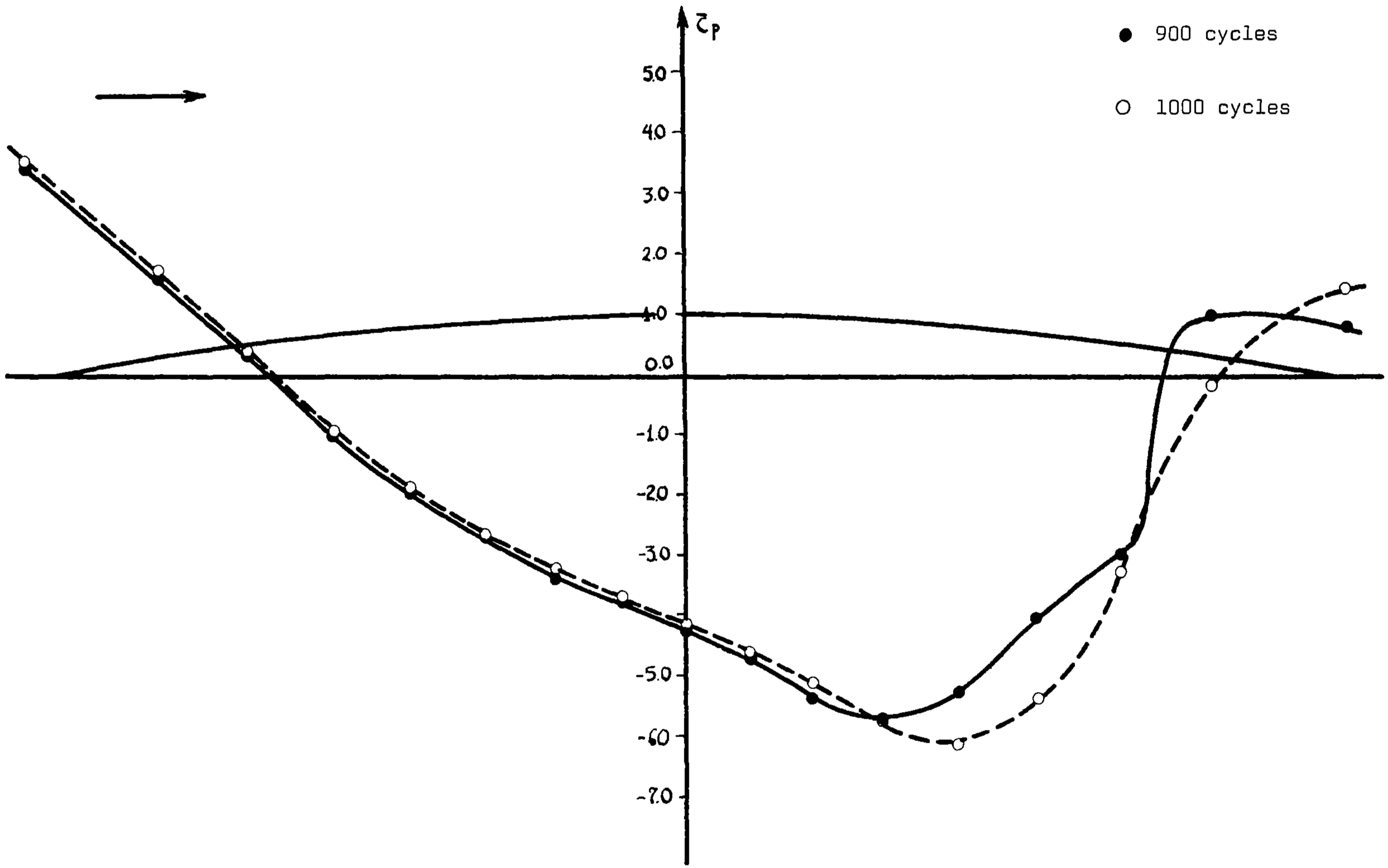

Figure 5. Transonic Pressure coefficient development in two-dimensional time varying flow. $M_o = 0.84$.

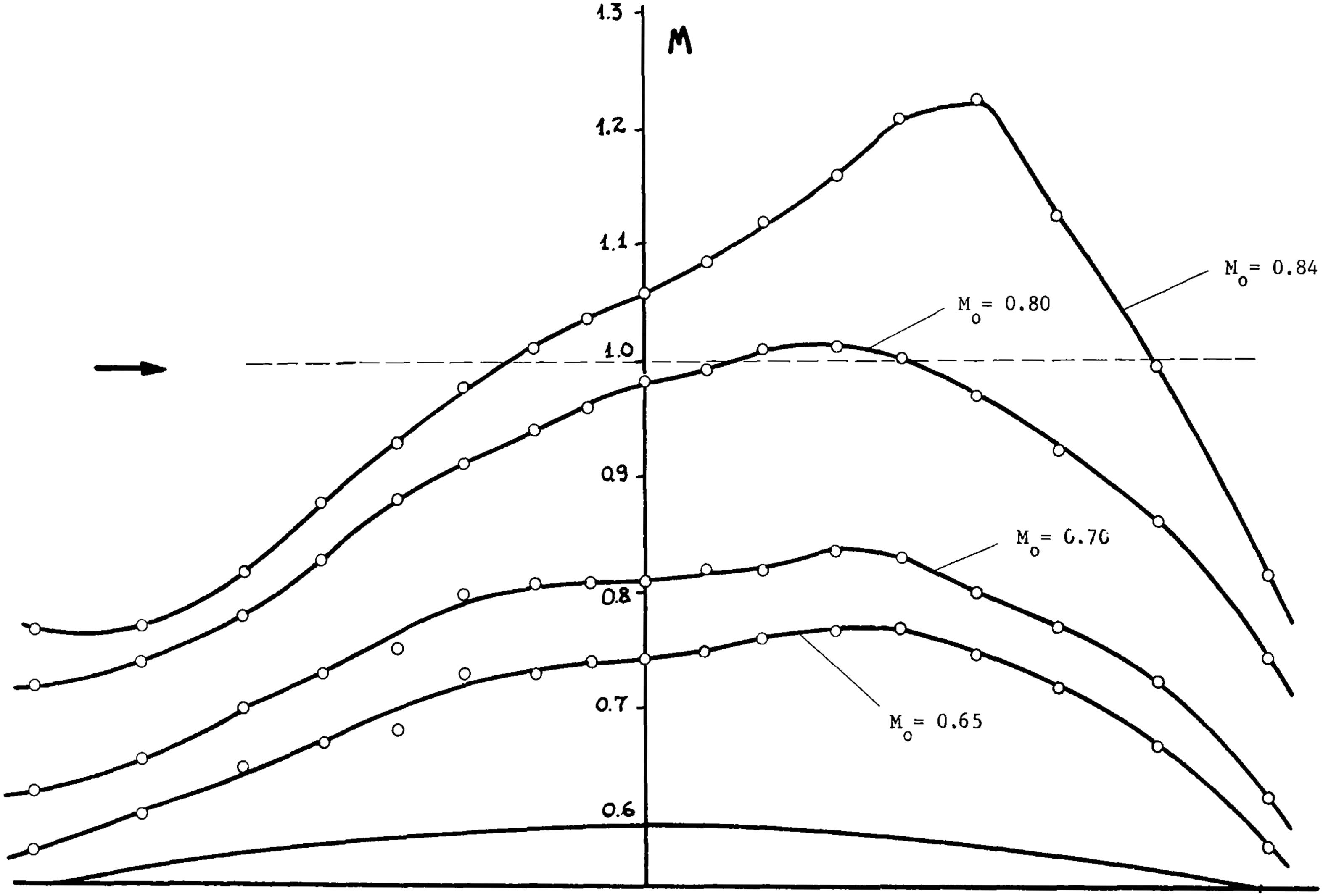

Figure 6. Mach number development in two-dimensional time varying flow.

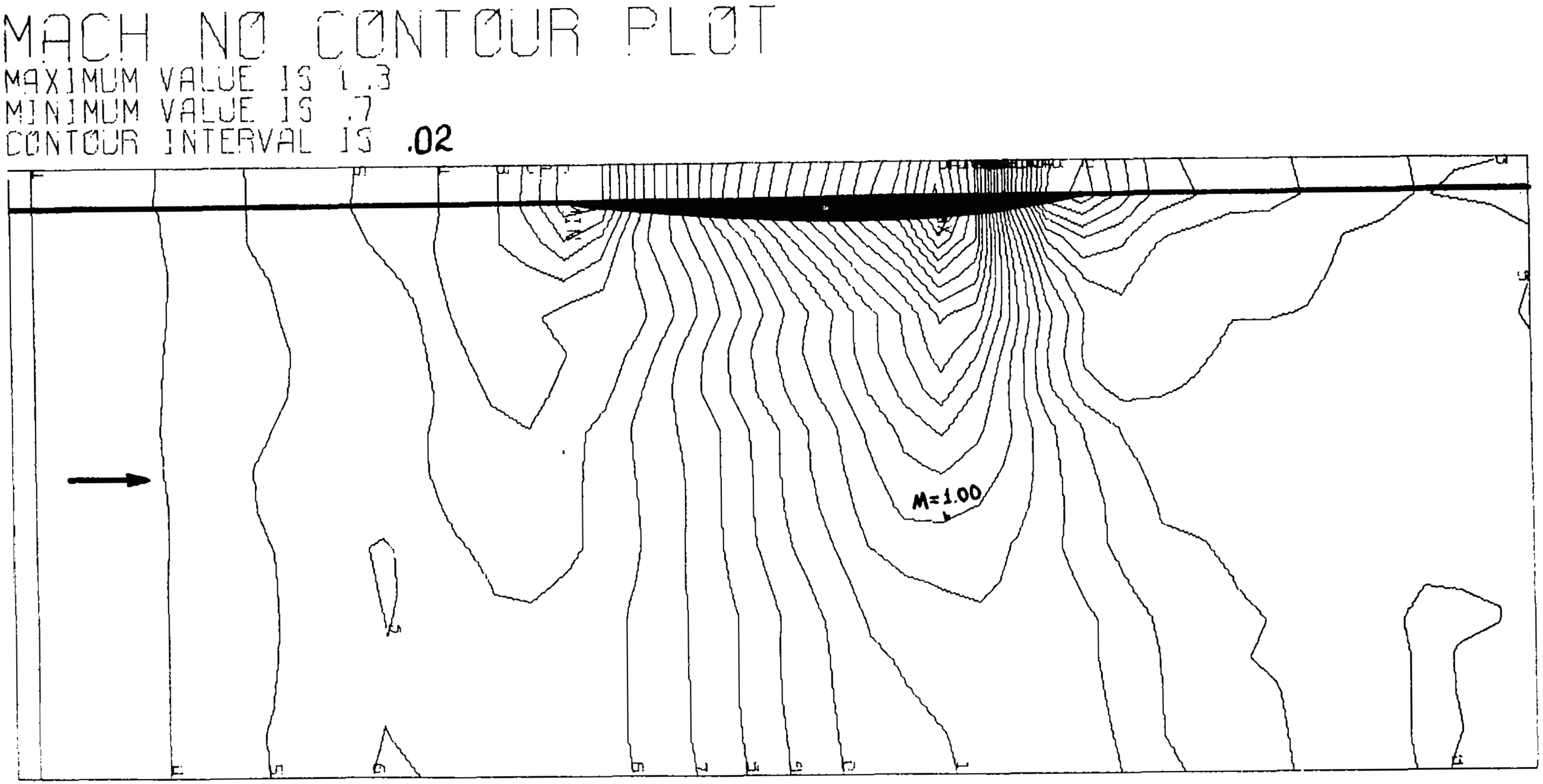

Figure 7. Mach number contours in time dependent two-dimensional flow at 1000 cycles. $M_o = 0.84$.

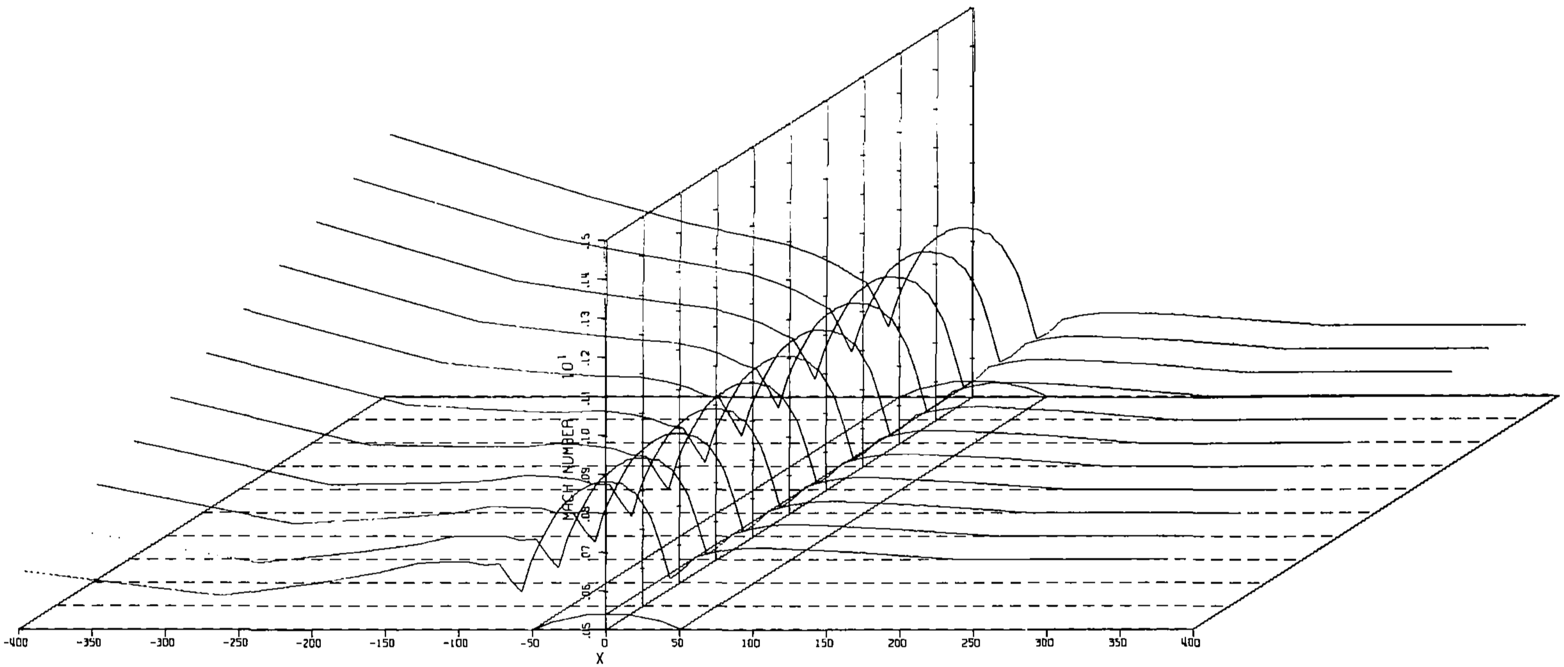

Figure 8. Mach number distribution in the plane of the blade at 300 cycles.

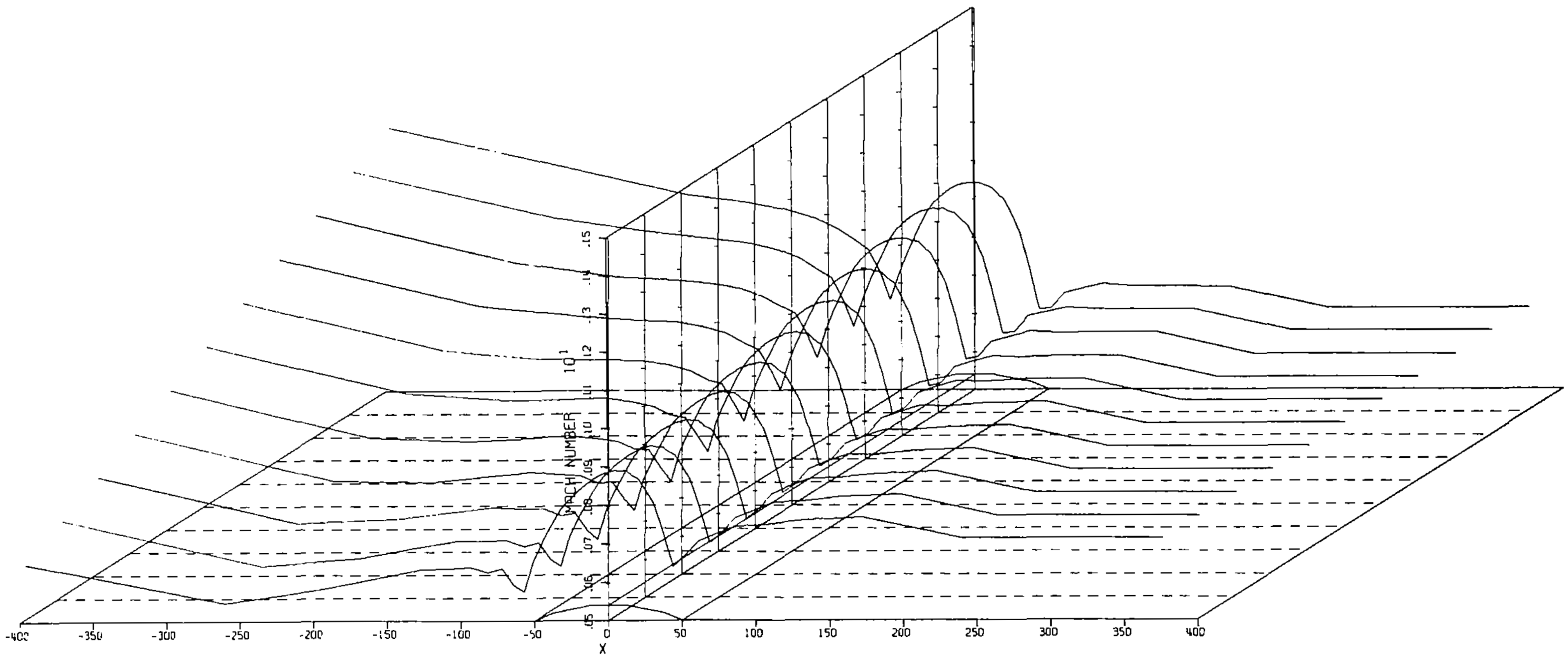

Figure 9. Mach number distribution in the plane of the blade at 400 cycles.

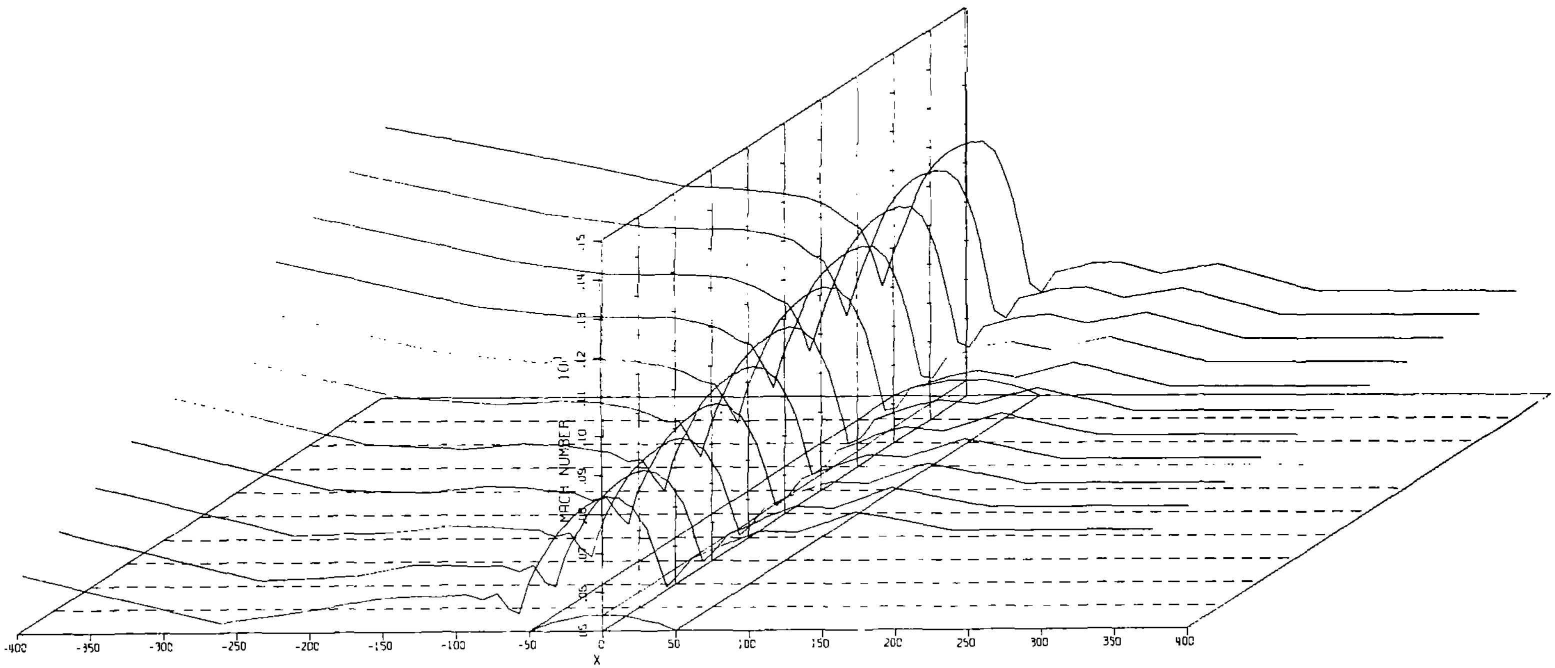

Figure 10. Mach number distribution in the plane of the blade at 500 cycles.

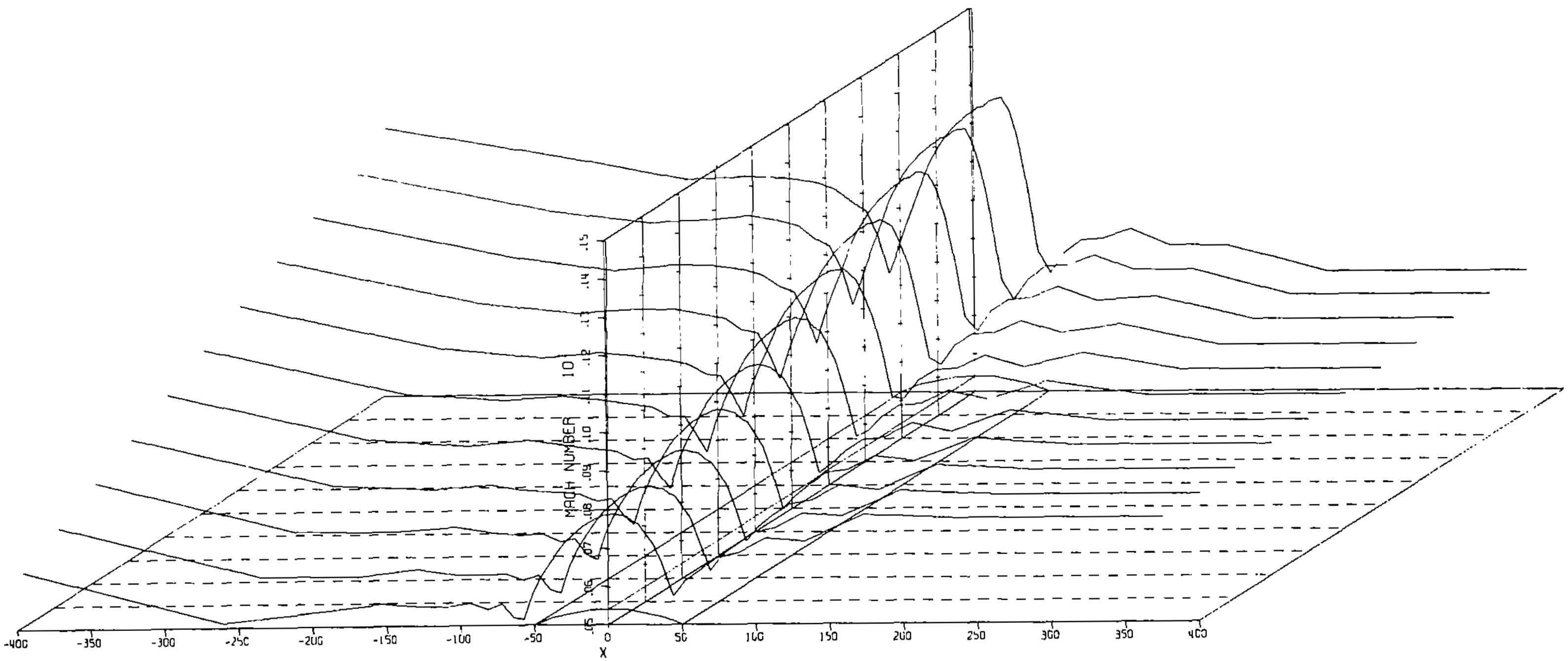

Figure 11. Mach number distribution in the plane of the blade at 600 cycles.

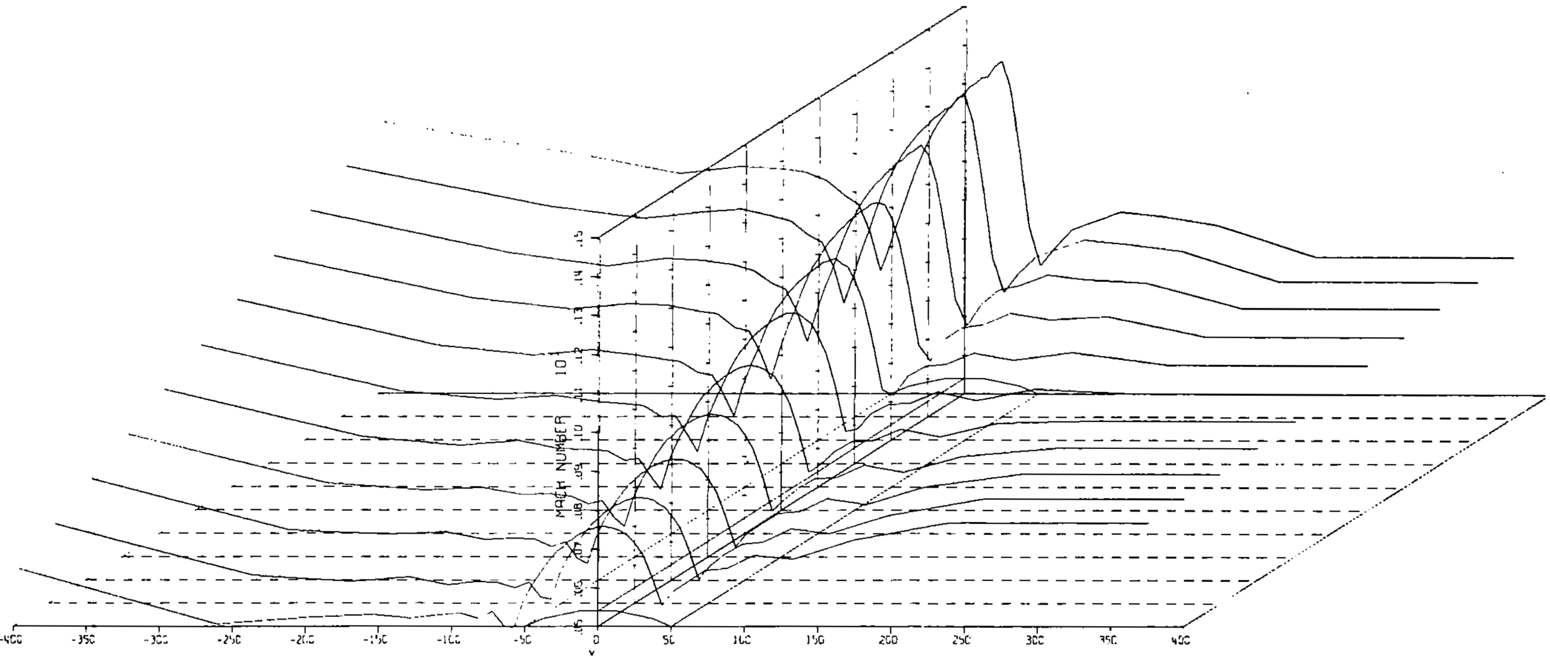

Figure 12. Mach number distribution in the plane of the blade at 700 cycles.

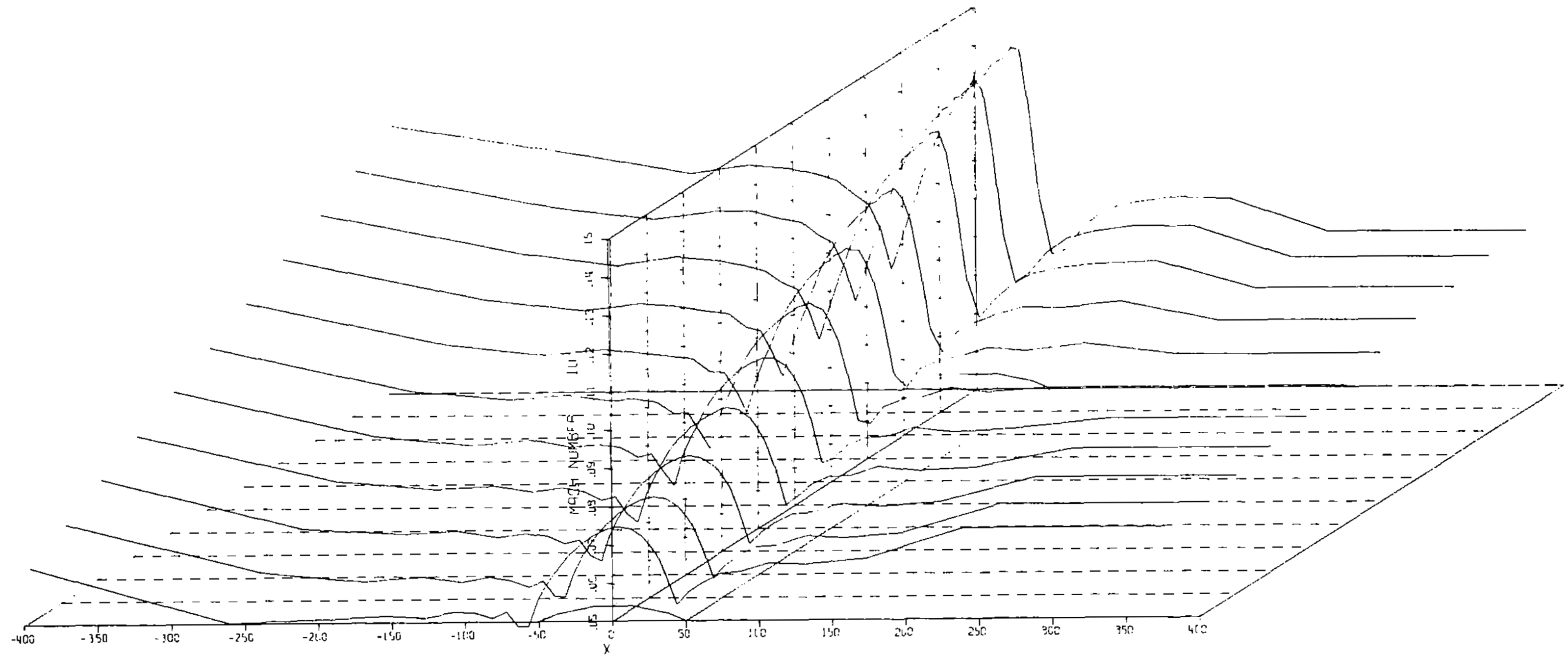

Figure 13. Mach number distribution in the plane of the blade at 800 cycles.

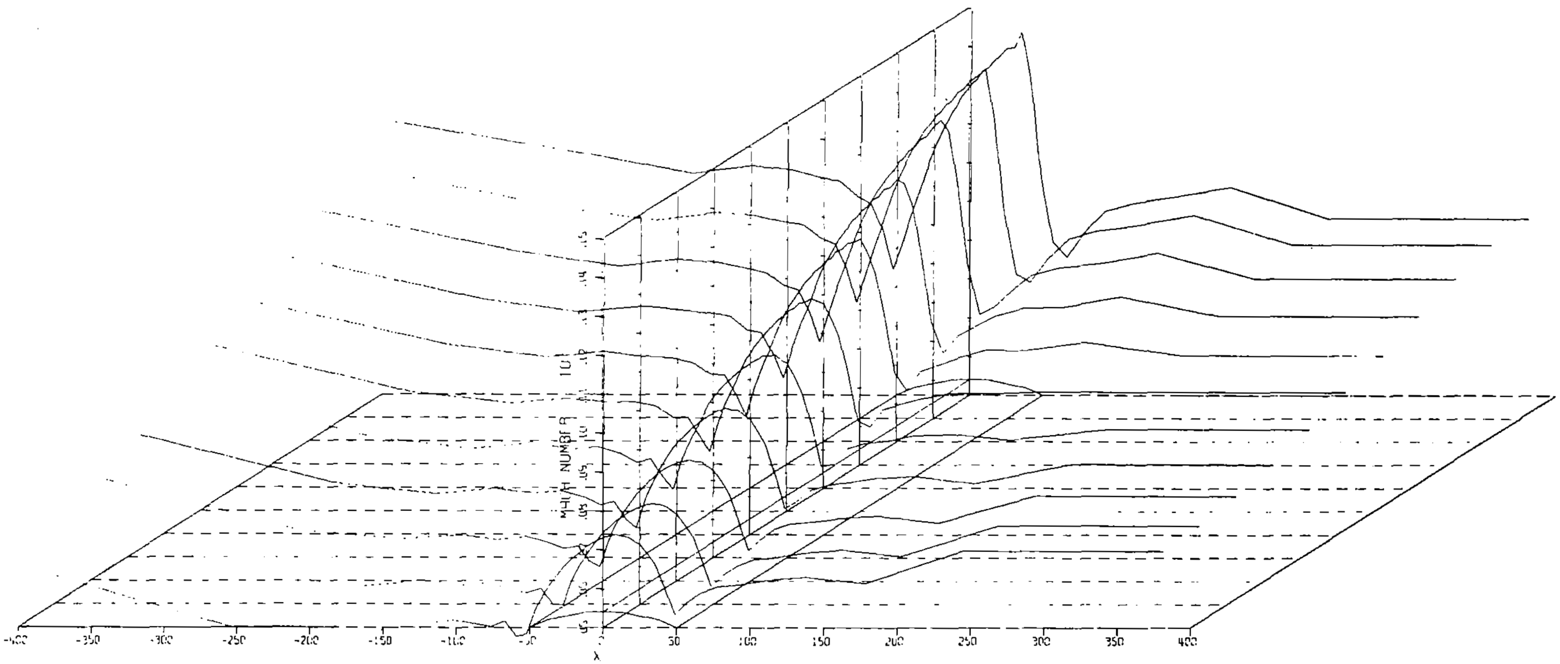

Figure 14. Mach number distribution in the plane of the blade at 900 cycles.

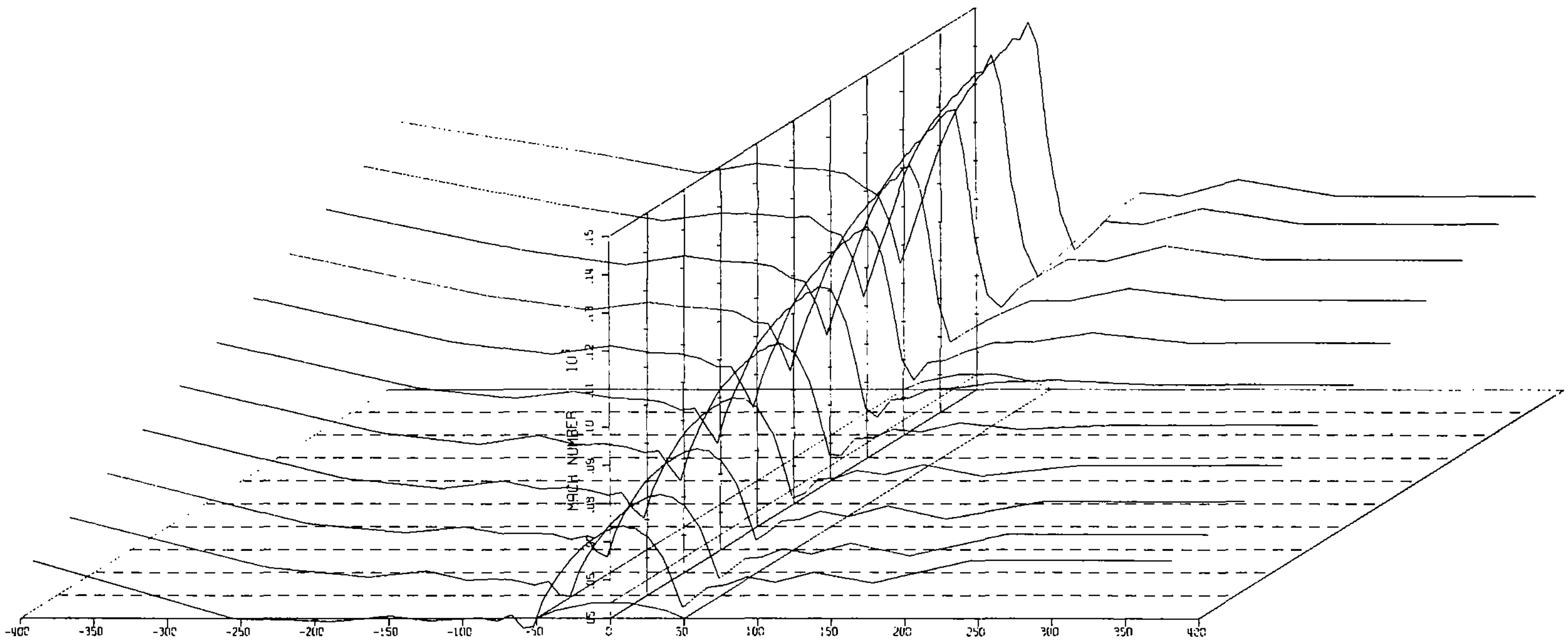

Figure 15. Mach number distribution in the plane of the blade at 1000 cycles.

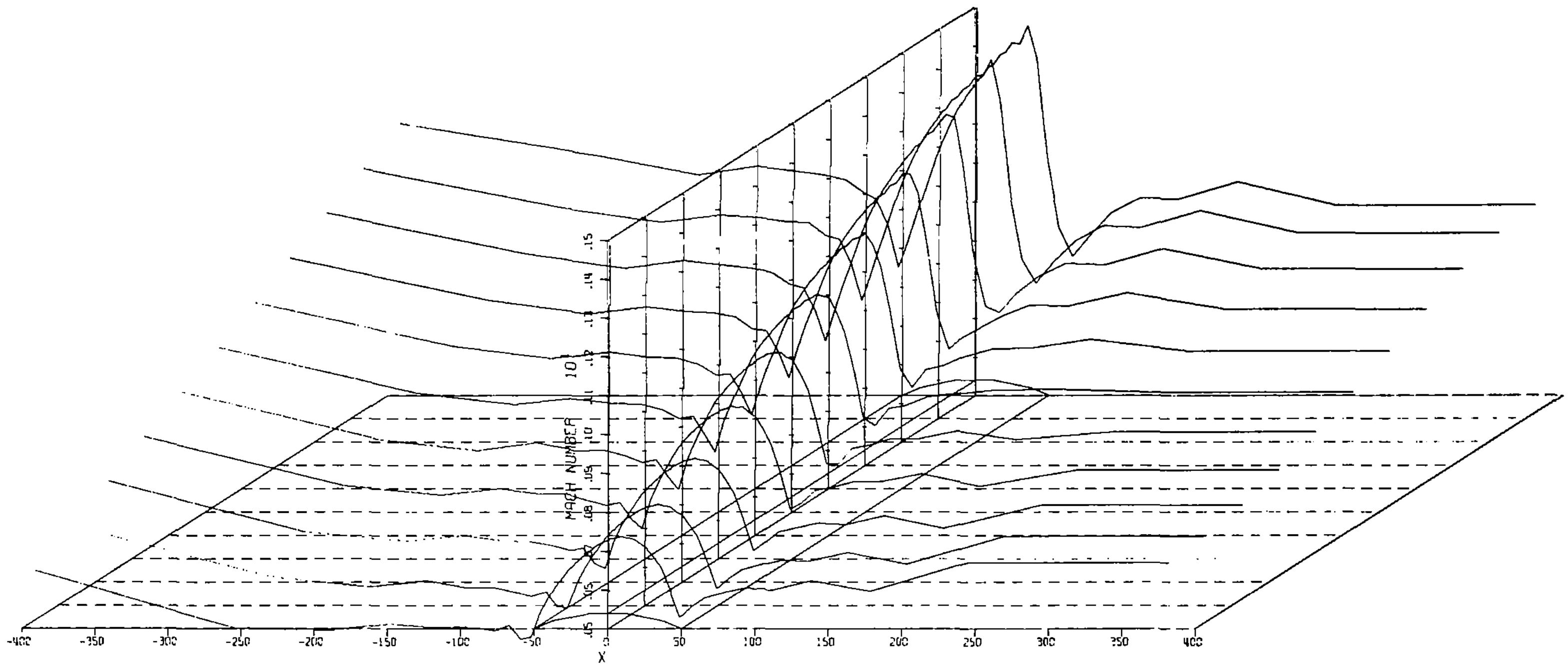

Figure 16. Mach number distribution in the plane of the blade at 1100 cycles.

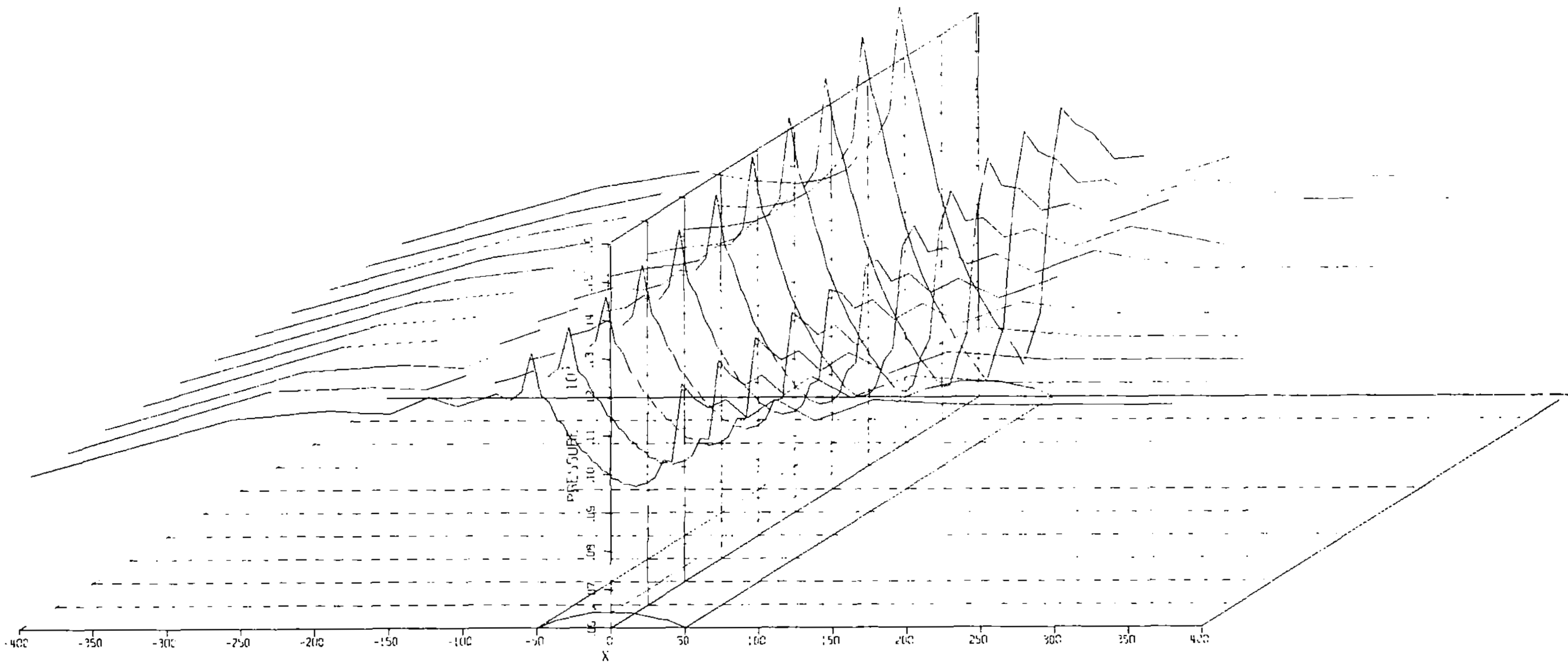

Figure 17. Static pressure distribution in the plane of the blade at 700 cycles.

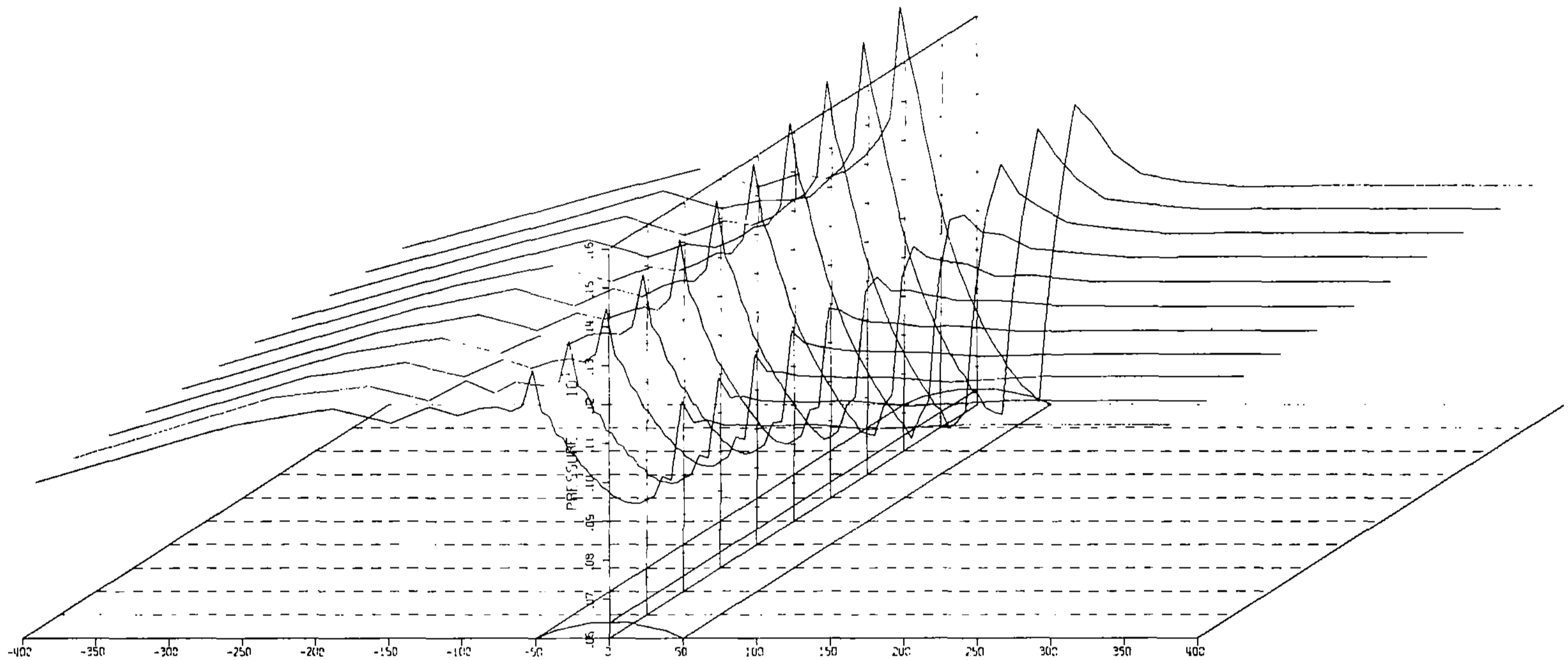

Figure 18. Static pressure distribution in the plane of the blade at 1100 cycles.

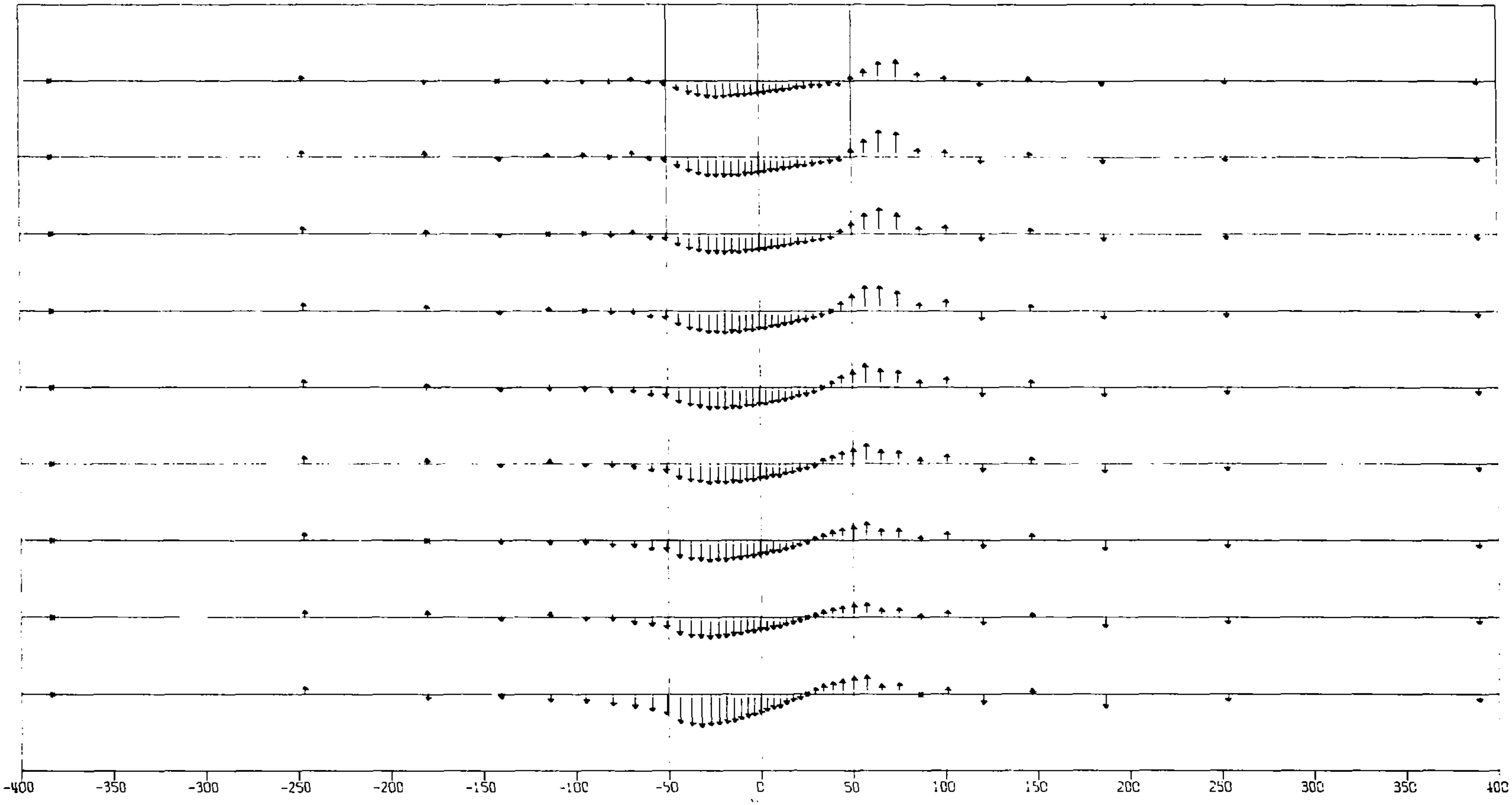

Figure 19. Cross flow distribution in the plane of the blade at 1100 cycles.

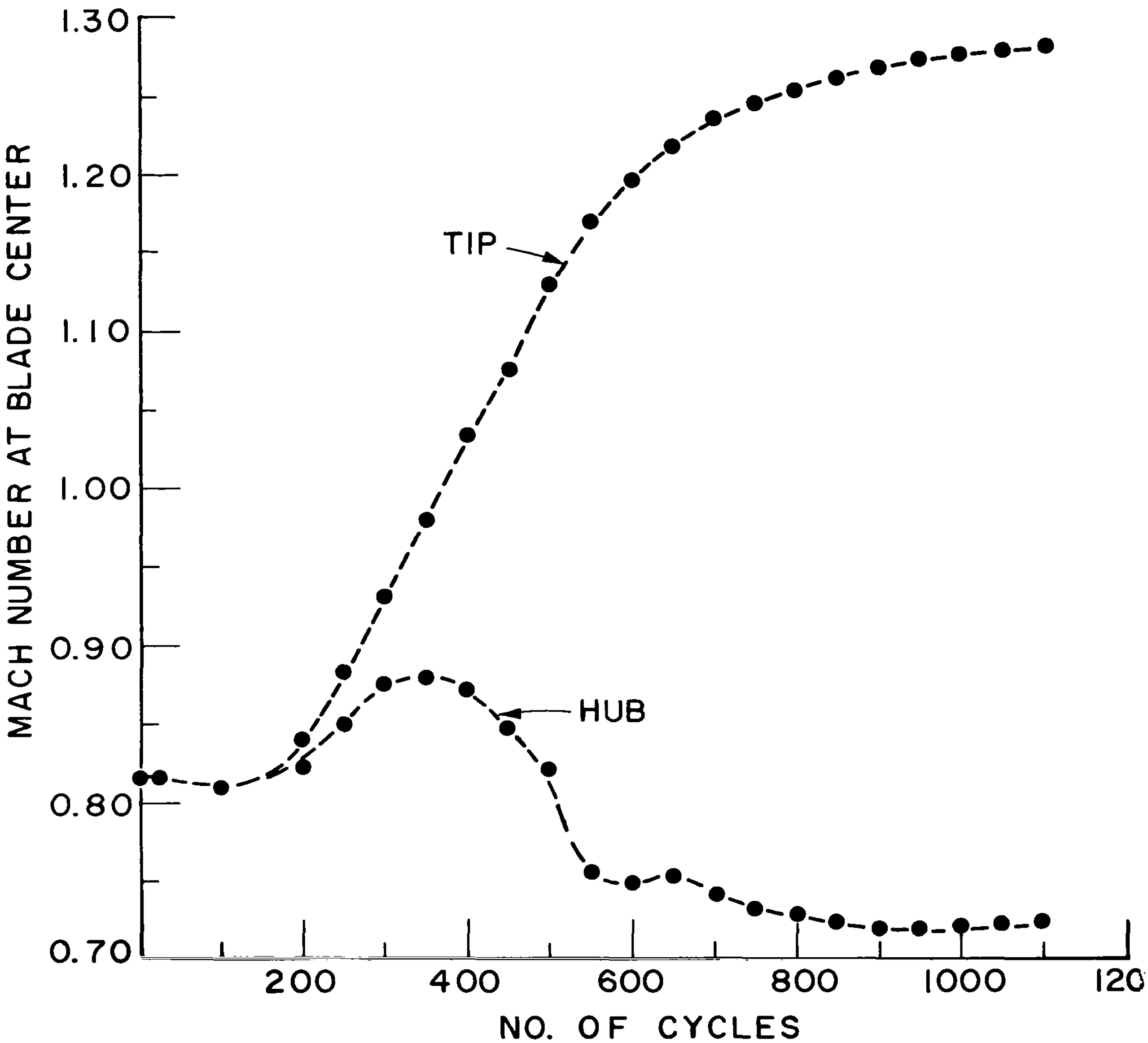

Figure 20. Mach number evolution at hub and tip. Note steady decrease of hub Mach number once shock forms at tip.